

ORIGINAL RESEARCH ARTICLE

Machine learning-based prediction of tumor volume changes in MRIdian-based adaptive radiotherapy for prostate cancer

Merve Konuk¹, Ziya Kemal¹, Ozan Toker¹, Serhat Aras^{2*}, Banu Atalar³, and Orhan İçelli¹¹Department of Physics, Science and Art Faculty, Yıldız Technical University, Istanbul, Türkiye²Department of Radiation Oncology, Haydarpaşa Numune Training and Research Hospital, University of Health Sciences, Istanbul, Türkiye³Department of Radiation Oncology, Faculty of Medicine, Acıbadem Mehmet Ali Aydınlar University, Istanbul, Türkiye

Abstract

Accurate prediction of inter-fractional tumor volume changes may improve the efficiency and personalization of magnetic resonance-guided adaptive radiotherapy in prostate cancer (PCa). This study investigates the feasibility of using machine learning algorithms to predict inter-fraction gross tumor volume (GTV) changes in PCa during adaptive radiotherapy (ART), aiming to identify the optimal similarity coefficient and model to improve ART decision-making. Retrospective magnetic resonance images from 22 PCa patients treated using the ViewRay MRIdian LINAC system were analyzed. The GTV of each patient was recorded before treatment (GTV₀) and during five fractions (GTV₁₋₅). Four different similarity coefficients—dice, Jaccard, Tanimoto, and Ochiai similarity coefficients (DSC, JSC, TSC, and OSC)—were calculated to evaluate inter-fractional GTV variations. Machine learning models—artificial neural networks (ANNs), extreme gradient boosting machine, random forests, classification and regression trees, and k-nearest neighbors—were trained with appropriate hyperparameters to predict tumor volume changes between fractions. Their predictive performances were compared to determine the most effective algorithm. The ANN model demonstrated superior performance in predicting GTV variations across treatment fractions. Among the similarity coefficients, DSC contributed most to predicting inter-fractional tumor volume changes, while OSC had the least impact. The ANN model achieved the highest predictive performance on the independent test dataset ($R^2 = 0.822$). These findings indicate that ANN models can successfully predict inter-fractional GTV variations in PCa, thereby providing valuable support for ART decision-making. Incorporating DSC-based similarity analysis may facilitate ART planning and improve clinical outcomes. The study supports integrating AI-based methods into the ART workflow.

Keywords: Prostate cancer; Adaptive radiotherapy; MRIdian LINAC; Gross tumor volume; Machine learning; Similarity coefficients

***Corresponding author:**
Serhat Aras
(serhat.aras@sbu.edu.tr)

Citation: Konuk M, Kemal Z, Toker O, Aras S, Atalar B, İçelli O. Machine learning-based prediction of tumor volume changes in MRIdian-based adaptive radiotherapy for prostate cancer. *Adv Radiother Nucl Med.* 2026;4(2):026040003.
doi: 10.36922/ARNM026040003

Received: January 22, 2026

Revised: March 12, 2026

Accepted: April 24, 2026

Published online: May 15, 2026

Copyright: © 2026 Author(s). This is an Open-Access article distributed under the terms of the Creative Commons Attribution License, permitting distribution, and reproduction in any medium, provided the original work is properly cited.

Publisher's Note: AccScience Publishing remains neutral with regard to jurisdictional claims in published maps and institutional affiliations.

1. Introduction

Prostate cancer is the second most common cancer in men and a leading cause of cancer-related deaths worldwide.¹ Radiotherapy remains a primary treatment modality for prostate cancer, offering effective tumor treatment while minimizing damage to surrounding healthy tissues.² Several studies have detected changes in tumor volume and in peripheral organs at risk during radiotherapy, leading to the development of adaptive radiotherapy (ART).³⁻¹² ART is an effective method for detecting and evaluating radiation-induced changes in the gross tumor volume (GTV) and organs at risk. This method involves re-imaging and re-optimization of the treatment plan, particularly focusing on the GTV, prior to each treatment fraction.

Recent advances in machine learning and artificial intelligence (AI) have provided new opportunities for ART decision-making. Various AI-driven models have been developed to predict GTV changes, optimize treatment planning, and automate segmentation processes.¹³⁻¹⁹ Machine learning algorithms have demonstrated their potential in predicting when ART is required, reducing unnecessary plan modifications while ensuring precise dose delivery.²⁰⁻²⁸ Studies have utilized machine learning algorithms to predict the need for ART. Rachi *et al.*²⁸ developed a machine learning-based framework for ART decision-making in head and neck cancer, achieving an accuracy of over 90% in predicting ART requirements. Similarly, Nasief *et al.*²⁵ developed a machine learning model that uses data from the magnetic resonance (MR)-linear accelerator (LINAC) device to decide whether online ART is necessary for pancreatic cancer. Parchur *et al.*²⁷ developed a machine learning model to predict the need for daily online ART in pancreatic cancer, using the similarity index measure and entropy changes, achieving an area under the curve (AUC) of 0.93. However, machine learning-based studies aimed at predicting the need for ART in prostate cancer remain limited. Most existing research focuses on head and neck, lung, and pancreatic cancers, and there is currently no sufficiently comprehensive model for predicting ART necessity in prostate cancer.

Existing studies primarily focus on tumor volume tracking and segmentation rather than directly predicting the need for ART. In the present study, we evaluated the performance of five different machine learning algorithms (artificial neural networks [ANNs], extreme gradient boosting machine [XGBM], random forests, classification and regression trees [CART], and k-nearest neighbors [KNNs]) in predicting GTV changes in prostate cancer patients undergoing ART. In addition, we determined which of the dice, Jaccard, Tanimoto, and Ochiai similarity

coefficients (DSC, JSC, TSC, and OSC) is most effective in assessing inter-fractional GTV change in prostate cancer.

Although ART applications for prostate cancer have significantly advanced in recent years, accurately and reliably modeling inter-fractional changes in tumor volume remains an unmet clinical need. While the literature contains several machine learning-based predictive frameworks for head and neck, lung, and pancreatic cancers, comprehensive approaches directly addressing tumor volume variations in prostate cancer are scarce. Most existing studies have primarily focused on tumor volume tracking or image segmentation, rather than on establishing predictive decision-support mechanisms capable of proactively identifying the necessity of ART. The originality of our study lies in the quantitative evaluation of volumetric parameters derived from retrospective MR images using multiple similarity coefficients (DSC, JSC, TSC, and OSC), and in the systematic assessment of these features across five different machine learning algorithms (ANN, XGBM, random forest, CART, and KNN). By employing volume-based numerical dissimilarity measures instead of relying solely on complex image-processing methodologies, our study introduces a novel and streamlined approach to modeling inter-fractional variations.

The central hypothesis of this research is that ANNs, particularly when trained with DSC-based similarity metrics, can outperform other algorithms in predicting prostate cancer tumor volume changes across treatment fractions, thereby offering a more accurate and generalizable framework for ART decision-making. This predictive capability has the potential to minimize unnecessary replanning, optimize personalized dose distribution, and ultimately enhance treatment efficiency for individual patients. In this context, our work contributes not only by comparing algorithmic performances and similarity measures but also by proposing a clinically applicable model that integrates AI directly into ART workflows. Thus, the present study provides radiation oncologists and medical physicists with a new perspective on ART planning, emphasizing a predictive and patient-specific strategy that may significantly improve treatment precision and clinical outcomes.

The aim of this study is to compare the performance of different similarity coefficients and machine learning algorithms in predicting potential inter-fractional GTV changes in ART for prostate cancer.

2. Materials and methods

This study analyzed retrospective MR images of 22 prostate cancer patients, each image treated in five fractions, using

an MRIdian LINAC system (ViewRay, United States [US]) (Table 1). MR images were acquired using the integrated 0.35-T MRI unit of the ViewRay MRIdian LINAC system and were retrieved retrospectively from the MRIdian treatment planning system (Department of Radiation Oncology, Faculty of Medicine, Acibadem Mehmet Ali Aydınlar University, Istanbul, Türkiye).

2.1. Calculation of similarity values

Dice similarity coefficient, JSC, TSC, and OSC were used to analyze the change between volumes. Their calculations are as follows:

- (i) Dice similarity coefficient²⁹ is used to measure the level of agreement between two segmentations. Let A and B be the target regions for the DSC calculation. Criterion of similarity between target regions:

$$DSC(A, B) = \frac{2(A \cap B)}{A + B} \quad (1)$$

- (ii) Jaccard similarity coefficient³⁰ expresses the intersection of two sets divided by their union. Its mathematical representation is:

$$JSC(A, B) = \frac{A \cap B}{A \cup B} = \frac{A \cap B}{A + B - (A \cap B)} \quad (2)$$

- (iii) Tanimoto similarity coefficient³¹ is formalized using statistical decision theory, measuring true positive (TP), true negative (TN), false positive (FP), and false negative (FN):

$$TSC(A, B) = \frac{TP}{TP + FP + FN} = \frac{|A \cap B|}{|A - B| + |B - A| + (A \cap B)} \quad (3)$$

- (iv) Ochiai similarity coefficient (also known as Ochiai Otsuka similarity)³² is calculated as follows:

$$OSC(A, B) = \frac{|A \cap B|}{\sqrt{|A| \cdot |B|}} \quad (4)$$

Here, $|A \cap B|$ represents the intersection of two sets, and $\sqrt{|A| \cdot |B|}$ represents the square root of the product of the two sets. DSC, JSC, TSC, and OSC take values between 0 and 1. When the value is close to zero, the similarity is low; when it is close to one, the similarity is high.

In this study, GTV was defined as the entire prostate gland contoured on MR images within the MRIdian LINAC treatment planning system. All analyses were conducted based on whole-prostate volumes. All prostate contours were delineated using a single experienced radiation oncologist in accordance with institutional contouring protocols. No multiple independent contour sets were generated, and no contour averaging was performed. All prostate delineations and inter-fraction comparisons were performed on T2-weighted MR images acquired with

the MRIdian LINAC system (0.35 Tesla). Imaging was conducted using the system's integrated MR imaging unit with a standard abdominal surface coil configuration. No endorectal coil was used during image acquisition. The same imaging protocol was applied for baseline and all treatment fractions to ensure consistency in volumetric comparisons.

The models were not designed to predict GTV₅ using the similarity between GTV₀ and GTV₄. Each fraction was analyzed independently, and the similarity coefficient between GTV₀ and the corresponding fraction was used to model the volume change of that specific fraction. All patients were treated with a five-fraction stereotactic body radiotherapy protocol using the MRIdian LINAC system. Therefore, analyses were performed based on five treatment fractions in accordance with the clinical treatment scheme. Initially, GTV₀ was plotted and recorded in the MRIdian LINAC treatment planning system before treatment. Then, the GTV₁ in the first fraction, GTV₂ in the second fraction, GTV₃ in the third fraction, GTV₄ in the fourth fraction, and GTV₅ in the fifth fraction were plotted for each patient and recorded in the system. The intersection volumes of GTV₀ ∩ GTV₁, GTV₀ ∩ GTV₂, GTV₀ ∩ GTV₃, GTV₀ ∩ GTV₄, and GTV₀ ∩ GTV₅ were generated for the intersection values using Equations 1–4. GTVs recorded in the treatment planning system for each patient were used to calculate DSC, JSC, TSC, and OSC, based on the volumes of the intersection and union.

2.2. Development of machine learning models

This study employed several machine learning algorithms, including ANN, XGBM, random forest, CART, and KNN.

2.2.1. Machine learning pipeline and training procedure

All analyses were performed using Python (version 3.9; Python Software Foundation, US) with the scikit-learn and XGBoost libraries. For each patient, intersection volumes between baseline GTV₀ and fraction-specific GTV₁₋₅ were extracted from the treatment planning system. These intersection volumes were used to compute four similarity coefficients (DSC, JSC, TSC, and OSC).

The similarity coefficients, together with the corresponding GTV volumetric measurements, were used as input features for the machine learning models. Continuous variables were standardized prior to modeling using StandardScaler, and no missing data were present in the dataset.

The dataset was divided into training (85%) and test (15%) subsets using patient-level splitting to prevent intra-patient data leakage. All models were trained exclusively on

the training dataset using the predefined hyperparameters reported in [Table 2](#). Hyperparameters were selected based on preliminary experiments and prior literature to achieve stable model performance.

Model performance was evaluated on the independent test dataset using regression metrics, including the coefficient of determination (R^2). These metrics were calculated for both the training and independent test datasets to assess model performance and generalization. Overfitting was assessed by comparing training and test performance metrics and by analyzing learning curves describing model performance across varying training set sizes. Feature importance analysis, where applicable, was used to assess the relative contribution of the similarity coefficients (DSC, JSC, TSC, and OSC) to the predictive models. The entire analytical workflow was implemented using a consistent and reproducible pipeline.

2.2.2. Data splitting and leakage prevention

To minimize the risk of data leakage and ensure statistical validity, dataset splitting was performed at the patient level rather than the observation level. All fraction-specific measurements belonging to a single patient were assigned exclusively to either the training or the test set, preventing information from the same patient from appearing in both subsets and eliminating intra-patient dependency leakage.

The dataset was divided into 85% for the training set and 15% for the test set using patient-level splitting. All preprocessing steps, including feature calculation and normalization, were performed after the train-test split and applied independently to each dataset. The test set was strictly held out and used only for final model evaluation.

2.3. Model validation strategy and prediction task definition

Model validation was performed at the patient level to ensure that model evaluation reflected performance on previously unseen patients. The predictive modeling task was formulated as a regression problem in which continuous inter-fractional GTV changes were estimated. The target variable for the regression models was defined as the inter-fractional GTV change relative to the baseline volume (Δ GTV).

3. Results

All DSC, JSC, TSC, and OSC were calculated using the GTV change values obtained in each treatment fraction. Using these similarity coefficients and inter-fraction GTV change values for prostate cancer, five machine learning models were developed, including ANN, XGBM, random forest, CART, and KNN.

In this study, the performance of different machine learning algorithms was analyzed. The relationship between training and test performance was examined to evaluate the generalization ability of the models. Therefore, both the training and test performances were examined to determine whether the five models used in the study were appropriately trained and how well they performed on new data.

As shown in [Table 3](#), the training R^2 values of the five models ranged from 0.948 to 0.985, indicating that all machine learning algorithms performed well on the training sets. Random forest achieved the highest training R^2 value (0.985) but showed a lower performance on the test dataset ($R^2 = 0.696$) compared to other models. These results indicate that random forest may perform weaker than the other algorithms when applied to new data. A notable difference between the training and test performances of the random forest model was observed compared to the other algorithms. This discrepancy suggests the model may be overfitting, given its high training performance.

The ANN model had the lowest training R^2 value (0.948) but achieved the highest test R^2 value (0.822). It was also observed that the difference between the training and test performances of the ANN was smaller than that of the other algorithms. When the training and test performances were considered together, the ANN model appeared to be effectively trained, as the results across both datasets were relatively close. The ANN model, therefore, demonstrated better generalization performance than the other models. In contrast, the XGBM model achieved a high training R^2 value (0.977), while its performance on the test dataset was comparatively lower.

The KNN and CART models demonstrated lower predictive performance compared with other algorithms. Their performance on the training and test sets was similar. The performance of the models, measured by R^2 score, across different training set sizes is shown in [Figure 1](#). The R^2 learning curve illustrates how model performance changes as the amount of training data increases. The results indicate that although the XGBM model performed well on the training set, the ANN model achieved the best predictive performance on the test set. Furthermore, the R^2 curve shows that the ANN maintained relatively stable predictive performance across the range of training set sizes. This suggests that while some algorithms become more susceptible to overfitting as the training set size increases, the ANN model provides stable predictive capability.

A model feature importance analysis was performed to determine which of DSC, JSC, TSC, and OSC contributed most to the predictive models. DSC showed the greatest

contribution among the similarity features, exerting a greater influence on the algorithms than other similarity coefficients (Figure 2). Among the models, ANN was the most prominent model. In addition, OSC had the lowest contribution. Therefore, the OSC values were removed

from the dataset, and the models were rebuilt. However, Figure 3 shows a slight decrease in OSC prediction performance. Although OSC had a lower importance score, removing it from the dataset slightly reduced the predictive performance, indicating that it still contributed to the model.

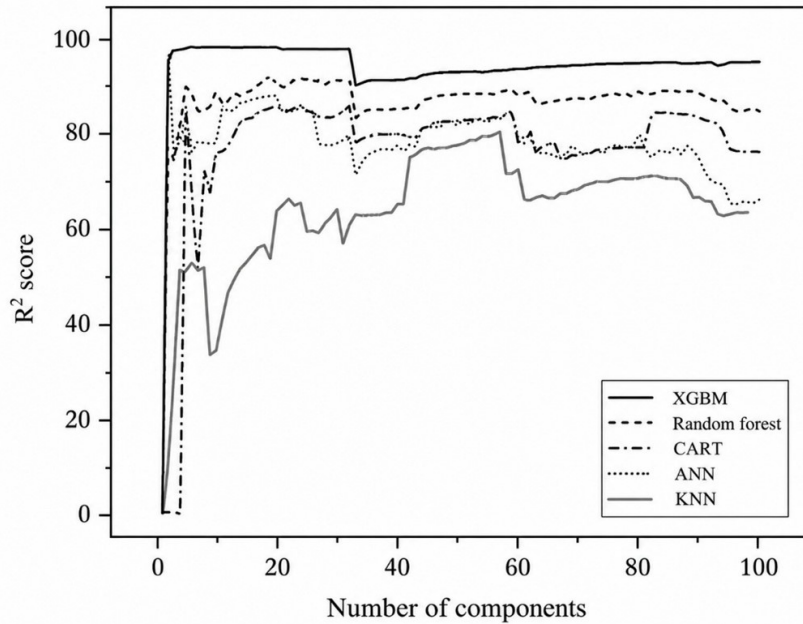


Figure 1. Success rates for machine learning algorithms as the training size changes
 Abbreviations: ANN: Artificial neural network; CART: Classification and regression trees; KNN: K-nearest neighbor; XGBM: Extreme gradient boosting machine.

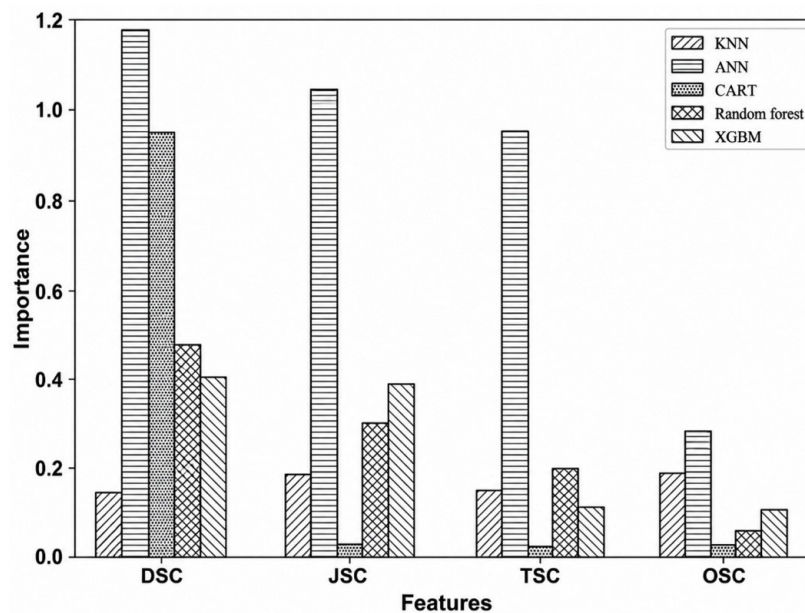


Figure 2. Feature importance for machine learning algorithms
 Abbreviations: ANN: Artificial neural network; CART: Classification and regression trees; DSC: Dice similarity coefficient; JSC: Jaccard similarity coefficient; KNN: K-nearest neighbor; OSC: Ochiai similarity coefficient; TSC: Tanimoto similarity coefficient; XGBM: Extreme gradient boosting machine.

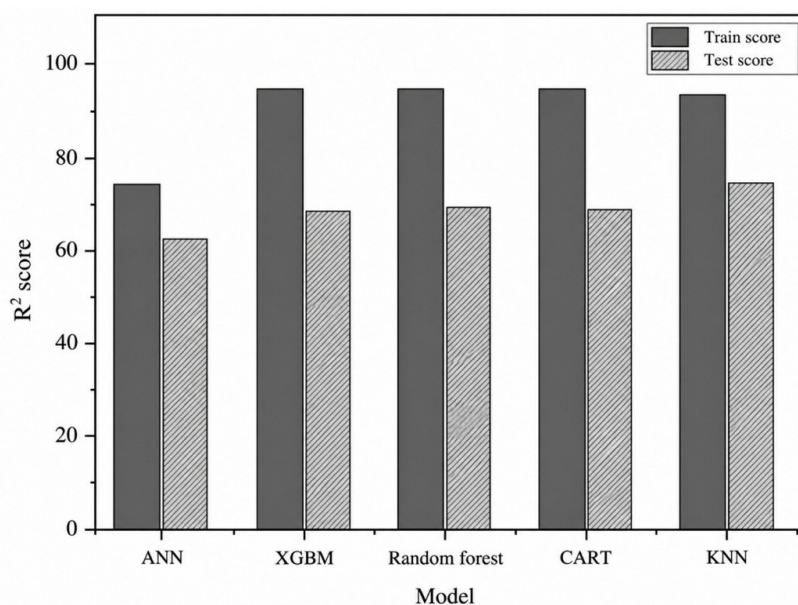


Figure 3. The performance of machine learning algorithms after removing the Ochiai similarity coefficient from the dataset
Abbreviations: ANN: Artificial neural network; CART: Classification and regression trees; KNN: K-nearest neighbor; XGBM: Extreme gradient boosting machine.

Table 1. Summary of baseline and inter-fractional GTV variations in prostate cancer

Fraction	Mean GTV (cm ³)	ΔGTV (cm ³) ^a	Relative change (%) ^b	SD (cm ³)
GTV ₀ (Baseline)	61.61	-	-	21.81
GTV ₁	60.75	-0.86	-1.40	21.07
GTV ₂	61.29	-0.32	-0.52	20.98
GTV ₃	61.89	+0.28	+0.45	20.60
GTV ₄	62.38	+0.77	+1.25	21.59
GTV ₅	62.20	+0.59	+0.96	20.86

Notes: ^aΔGTV = Mean GTV_n - Mean GTV₀; ^bRelative change (%) = $\frac{GTV_n - GTV_0}{GTV_0} \times 100$; ΔGTV and relative change values were calculated relative to the GTV₀ mean (61.61 cm³) using fraction means.
Abbreviation: GTV: Gross tumor volume.

4. Discussion

According to the study results, among the five machine learning algorithms trained with appropriate hyperparameters, ANN achieved the highest performance. The evaluation metrics demonstrate that ANN outperformed the other models in terms of predictive performance and generalization, making it the most effective model in this study. As a result, ANN appeared to be the most suitable algorithm among the evaluated models. In this study, where similarity measures were compared, DSC showed the strongest contribution among the evaluated metrics. This indicates that DSC is important for reliable predictions in treatment planning and that it

may serve as a valuable parameter in clinical applications. As a result, by estimating GTV changes in each treatment fraction in prostate cancer, this approach may help determine which treatment fractions could benefit from ART at the beginning of treatment.

Such approaches may provide practical support for radiation oncologists and medical physicists during the treatment planning process. In addition, understanding the radiotherapy response of GTV (tumor shrinkage, growth, displacement, etc.) may facilitate adaptation of the radiotherapy plan at different treatment stages and improve treatment delivery. In this way, this approach may improve radiotherapy response and treatment efficacy when potential GTV changes occur.

Table 2. Hyperparameters used in machine learning algorithms

Machine learning models	Hyperparameters	Values
ANN	alpha	0.1
	hidden layer sizes	300, 200, 150
XGBM	colsample_bytree	0.5
	learning_rate	0.01
	max_depth	2
	n_estimators	1000
Random forest	max_depth	6
	max_features	3
	n_estimators	500
CART	max_leaf_nodes	11
	min_samples_split	5
KNN	n_neighbors	3

Abbreviations: ANN: Artificial neural network; CART: Classification and regression trees; KNN: K-nearest neighbor; XGBM: Extreme gradient boosting machine.

Table 3. Training and testing R^2 values of machine learning algorithms

Machine learning models	Training R^2	Testing R^2
ANN	0.948	0.822
XGBM	0.976	0.725
Random forest	0.985	0.696
CART	0.964	0.703
KNN	0.957	0.766

Abbreviations: ANN: Artificial neural network; CART: Classification and regression trees; KNN: K-nearest neighbor; XGBM: Extreme gradient boosting machine.

The findings of this study align with previous research highlighting the potential of machine learning applications in ART. In the literature, various machine learning-based modeling approaches have been proposed to enhance decision-support processes in ART.^{21,25,27,28} For example, Thomas *et al.*³³ employed ANN models to predict intra-fraction dose distributions in MR-guided therapy and reported consistent performance across fractions. Similarly, the superior predictive performance of the ANN algorithm on the test set observed in this study is consistent with prior findings by Kai *et al.*³⁴ and Khalifa *et al.*¹⁷ which emphasize the high generalization capability of ANNs. In this context, ANN models appear to be a promising tool for modeling complex structural variations in radiotherapy planning.

Unlike previous studies using image processing techniques, this study focuses on geometric and morphological changes and uses only volume-based numerical similarity coefficients. This numerical approach enabled the prediction of GTV changes without complex

image processing. The ANN model demonstrated strong predictive performance when applied to this simplified data structure. Consequently, the study offers a streamlined, interpretable, and practically applicable modeling strategy as an alternative to image-based methods.

The findings of this study provide evidence that ANN demonstrates superior performance in predicting inter-fractional GTV changes in prostate cancer patients undergoing ART. Compared with other machine learning algorithms tested, including XGBM, random forest, CART, and KNN, ANN exhibited the highest test performance and the most balanced generalization between training and test sets, thereby minimizing the risk of overfitting. This outcome highlights the robustness of ANNs in handling the complex and nonlinear dynamics of tumor volume during radiotherapy. Importantly, the results also revealed that among the evaluated similarity coefficients, the DSC contributed most to predicting inter-fractional variations, whereas the OSC contributed least. These findings are

consistent with prior literature emphasizing the relevance of DSC in volumetric comparison and its clinical utility in treatment planning. Unlike several previous investigations that primarily focused on segmentation accuracy or geometric tracking, our study proposed a simplified and interpretable framework based on numerical similarity measures, thereby reducing reliance on computationally intensive image processing techniques.

The superior performance of the ANN model observed in this study may be explained by its ability to capture complex and nonlinear relationships between similarity coefficients and inter-fractional GTV variations. Tumor volume dynamics during ART are influenced by multifactorial geometric and anatomical changes that are unlikely to follow strictly linear or rule-based patterns. ANNs are universal function approximators capable of modeling nonlinear feature interactions and subtle dependencies among input variables. In our dataset, the similarity coefficients (DSC, JSC, TSC, and OSC) are mathematically related yet not identical, and their combined effects on volumetric variation may involve nonlinear interactions. The ANN architecture, with multiple hidden layers, is well-suited to learn such interaction effects without requiring explicit feature engineering. In contrast, tree-based models, such as random forests and CART, although flexible, tend to overfit, as reflected by larger discrepancies between training and test performance. This behavior may be attributable to the relatively limited sample size and the structured nature of the input features, which can lead to excessive model flexibility and increased variance. The ANN model, in comparison, exhibited a more balanced bias–variance trade-off and more stable generalization across varying training set sizes. These findings suggest that, under the present data structure, ANN provides a more robust modeling framework for capturing inter-fractional tumor volume dynamics in prostate ART.

The comparative analysis of different machine learning algorithms, the evaluation of model generalizability through overfitting assessment, the combined examination of various similarity coefficients, modeling based on real patient data, and the proposal of an approach that can directly contribute to clinical decision-making represent the main strengths of this study. This methodological novelty strengthens the translational potential of our results, as the predictive models can be more easily integrated into existing ART workflows. Nevertheless, certain limitations warrant consideration. Limitations of this study include the retrospective and single-institution design, the relatively small sample size of 22 patients, and the exclusive reliance on GTV changes without accounting for organs-at-risk dynamics, restricting the generalizability of the findings. Although patient-level

data splitting was used to reduce data leakage risk, the absence of external validation limits the strength of the conclusions. Furthermore, although the machine learning models used offer several advantages, they have inherent limitations such as overfitting, poor generalization, and computational inefficiency in large datasets. Additionally, only four similarity measures (DSC, JSC, TSC, and OSC) were evaluated; other potential measures were excluded. For these reasons, more comprehensive and multicenter studies are needed in the future. Moreover, while ANN outperformed other algorithms in this study, future investigations with larger and more heterogeneous patient cohorts are necessary to validate the scalability and clinical robustness of the model. Despite these limitations, the present study underscores the promise of machine learning-driven decision-support systems for personalized ART in prostate cancer, potentially enabling more efficient allocation of clinical resources, reducing unnecessary replanning, and improving treatment precision.

5. Conclusion

This study will serve as an important guide for future similar studies and for improving medical treatment processes. In addition, tumor volume changes can be predicted by machine learning algorithms during prolonged treatments such as hyperfractionation. This will provide significant practical benefits from the use of machine learning algorithms in long-term treatments and in situations where ART is difficult to apply. This study has been a source of inspiration for improving the treatment process. In our future studies, we plan to contribute to the treatment of diverse patient populations using machine learning algorithms by adding tumor volumes from the abdomen and thorax to the dataset.

Acknowledgments

During the preparation of this manuscript, the ChatGPT 5.1 language model developed by OpenAI was used solely to support English grammar correction, improve the clarity and coherence of scientific expression, and assist in translating the text into English. The all-data analysis, scientific interpretation, and content generation were conducted exclusively by the author(s).

Funding

None.

Conflict of interest

The authors declare that they have no known competing financial interests or personal relationships that could have appeared to influence the work reported in this paper.

Author contributions

Conceptualization: Merve Konuk, Ziya Kemal
Data curation: Merve Konuk
Formal analysis: Merve Konuk, Ziya Kemal, Ozan Toker
Investigation: Merve Konuk
Methodology: Merve Konuk, Ozan Toker
Project administration: Serhat Aras
Supervision: Serhat Aras
Validation: Banu Atalar, Orhan İçelli
Visualization: Ziya Kemal
Writing—original draft: Merve Konuk
Writing—review & editing: Ozan Toker, Serhat Aras, Banu Atalar, Orhan İçelli

Ethics approval and consent to participate

Ethical approval for this study was granted by the Acıbadem Mehmet Ali Aydınlar Üniversitesi Tıbbi Araştırmalar Değerlendirme Kurulu (ATADEK) (Approval No: ATADEK-2019/14).

Consent for publication

Not applicable.

Availability of data

The data used/provided in this study are explicitly stated in the manuscript and are available from the corresponding author upon reasonable request.

References

1. Sung H, Ferlay J, Siegel RL, *et al.* Global Cancer Statistics 2020: GLOBOCAN estimates of incidence and mortality worldwide for 36 cancers in 185 countries. *CA Cancer J Clin.* 2021;71(3):209-249.
doi: 10.3322/caac.21660
2. Sekhoacha M, Riet K, Motloung P, Gumenuk L, Adegoke A, Mashele S. Prostate cancer review: Genetics, diagnosis, treatment options, and alternative approaches. *Molecules.* 2022;27(17):5730.
doi: 10.3390/molecules27175730
3. Batista V, Richter D, Chaudhri N, Naumann P, Herfarth K, Jäkel O. Significance of intra-fractional motion for pancreatic patients treated with charged particles. *Radiat Oncol.* 2018;13(1).
doi: 10.1186/s13014-018-1060-8
4. Dial C, Weiss E, Siebers JV, Hugo GD. Benefits of adaptive radiation therapy in lung cancer as a function of replanning frequency. *Med Phys.* 2016;43(4):1787-1794.
doi: 10.1118/1.4943564
5. Finazzi T, Palacios MA, Haasbeek CJA, *et al.* Stereotactic MR-guided adaptive radiation therapy for peripheral lung tumors. *Radiother Oncol.* 2020;144:46-52.
doi: 10.1016/j.radonc.2019.10.013
6. Green OL, Henke LE, Hugo GD. Practical clinical workflows for online and offline adaptive radiation therapy. *Semin Radiat Oncol.* 2019;29(3):219-227.
doi: 10.1016/j.semradonc.2019.02.004
7. Li Y, Hoisak JDP, Li N, *et al.* Dosimetric benefit of adaptive re-planning in pancreatic cancer stereotactic body radiotherapy. *Med Dosim.* 2015;40(4):318-324.
doi: 10.1016/j.meddos.2015.04.002
8. Mannerberg A, Persson E, Jonsson J, *et al.* Dosimetric effects of adaptive prostate cancer radiotherapy in an MR-linac workflow. *Radiat Oncol.* 2020;15(1).
doi: 10.1186/s13014-020-01604-5
9. Nierer L, Eze C, da Silva Mendes V, *et al.* Dosimetric benefit of MR-guided online adaptive radiotherapy in different tumor entities: liver, lung, abdominal lymph nodes, pancreas and prostate. *Radiat Oncol.* 2022;17(1).
doi: 10.1186/s13014-022-02021-6
10. Rudra S, Jiang N, Rosenberg SA, *et al.* Using adaptive magnetic resonance image-guided radiation therapy for treatment of inoperable pancreatic cancer. *Cancer Med.* 2019;8(5):2123-2132.
doi: 10.1002/cam4.2100
11. Sonke JJ, Aznar M, Rasch C. Adaptive radiotherapy for anatomical changes. *Semin Radiat Oncol.* 2019;29(3):245-257.
doi: 10.1016/j.semradonc.2019.02.007
12. Yan D, Vicini F, Wong J, Martinez A. Adaptive radiation therapy. *Phys Med Biol.* 1997;42(1):123-132.
doi: 10.1088/0031-9155/42/1/008
13. Jeong S, Cheon W, Kim S, Park W, Han Y. Deep-learning-based segmentation using individual patient data on prostate cancer radiation therapy. *PLoS ONE.* 2024;19(7):e0308181.
doi: 10.1371/journal.pone.0308181
14. Derbal Y. Adaptive treatment of metastatic prostate cancer using generative artificial intelligence. *Clin Med Insights Oncol.* 2025;19:11795549241311408.
doi: 10.1177/11795549241311408
15. Hwang J, Eum H, Kim JS, Lee E, Kang BH, Park Y. Personalized deep learning model for target volume based on CBCT for prostate adaptive SBRT patients. *Int J Radiat Oncol Biol Phys.* 2024;120(2):e539-e540.
doi: 10.1016/j.ijrobp.2024.07.1196
16. Brand VJ, Milder MTW, Christianen MEMC, *et al.* First-in-men online adaptive robotic stereotactic body radiation

- therapy: toward ultrahypofractionation for high-risk prostate cancer patients. *Adv Radiat Oncol*. 2025;10(2):101701.
doi: 10.1016/j.adro.2024.101701
17. Khalifa A, Winter JD, Tadic T, Purdie TG, McIntosh C. Machine learning automated treatment planning for online magnetic resonance guided adaptive radiotherapy of prostate cancer. *Phys Imaging Radiat Oncol*. 2024;32:100649.
doi: 10.1016/j.phro.2024.100649
18. Radici L, Piva C, Casanova Borca V, *et al*. Clinical evaluation of a deep learning CBCT auto-segmentation software for prostate adaptive radiation therapy. *Clin Transl Radiat Oncol*. 2024;47:100796.
doi: 10.1016/j.ctro.2024.100796
19. Kim JI, Park JM, Choi CH, An HJ, Kim YJ, Kim JH. Retrospective study comparing MR-guided radiation therapy (MRgRT) setup strategies for prostate treatment: Repositioning vs. replanning. *Radiat Oncol*. 2019;14(1).
doi: 10.1186/s13014-019-1349-2
20. Ma C, Tian Z, Wang R, *et al*. A prediction model for dosimetric-based lung adaptive radiotherapy. *Med Phys*. 2022;49(10):6319-6333.
doi: 10.1002/mp.15714
21. Brown E, Owen R, Harden F, *et al*. Predicting the need for adaptive radiotherapy in head and neck cancer. *Radiother Oncol*. 2015;116(1):57-63.
doi: 10.1016/j.radonc.2015.06.025
22. Guidi G, Maffei N, Vecchi C, *et al*. A support vector machine tool for adaptive tomotherapy treatments: Prediction of head and neck patients criticalities. *Phys Med*. 2015;31(5):442-451.
doi: 10.1016/j.ejmp.2015.04.009
23. Guidi G, Maffei N, Meduri B, *et al*. A machine learning tool for re-planning and adaptive RT: A multicenter cohort investigation. *Phys Med*. 2016;32(12):1659-1666.
doi: 10.1016/j.ejmp.2016.10.005
24. Nasief H, Omari E, Zhang Y, *et al*. Automatically determining necessity of online adaptive replanning based on MRI wavelet multiscale texture features for MRI-guided adaptive radiation therapy. *Int J Radiat Oncol Biol Phys*. 2021;111(3):S55.
doi: 10.1016/j.ijrobp.2021.07.142
25. Nasief HG, Parchur AK, Omari E, *et al*. Predicting necessity of daily online adaptive replanning based on wavelet image features for MRI guided adaptive radiation therapy. *Radiother Oncol*. 2022;176:165-171.
doi: 10.1016/j.radonc.2022.10.001
26. Kavanaugh J, Roach M, Ji Z, Fontenot J, Hugo GD. A method for predictive modeling of tumor regression for lung adaptive radiotherapy. *Med Phys*. 2021;48(5):2083-2094.
doi: 10.1002/mp.14529
27. Parchur AK, Lim S, Nasief HG, *et al*. Auto-detection of necessity for MRI-guided online adaptive replanning using a machine learning classifier. *Med Phys*. 2023;50(1):440-448.
doi: 10.1002/mp.16047
28. Rachi T, Arijji T, Takahashi S. Development of machine-learning prediction programs for delivering adaptive radiation therapy with tumor geometry and body shape changes in head and neck volumetric modulated Arc therapy. *Adv Radiat Oncol*. 2023;8(4):101172.
doi: 10.1016/j.adro.2023.101172
29. Dice LR. Measures of the amount of ecologic association between species. *Ecology*. 1945;26(3):297-302.
doi: 10.2307/1932409
30. Jaccard P. The distribution of the flora in the alpine zone. *N Phytol*. 1912;11(2):37-50.
doi: 10.1111/j.1469-8137.1912.tb05611.x
31. Tanimoto TT. An elementary mathematical theory of classification and prediction. *Proc IBM Intern Rep*. Preprint posted online 1958.
32. Romesburg HC. *Cluster Analysis for Researchers*. Lifetime Learning Publications; 1984.
33. Thomas MA, Fu Y, Yang D. Development and evaluation of machine learning models for voxel dose predictions in online adaptive magnetic resonance guided radiation therapy. *J Appl Clin Med Phys*. 2020;21(7):60-69.
doi: 10.1002/acm2.12884
34. Kai Y, Arimura H, Ninomiya K, *et al*. Semi-automated prediction approach of target shifts using machine learning with anatomical features between planning and pretreatment CT images in prostate radiotherapy. *J Radiat Res*. 2020;61(2):285-297.
doi: 10.1093/jrr/rrz105